Bull. Mater. Sci. (2022)45:77
https://doi.org/10.1007/s12034-021-02653-6

Synthesis and characterization of CdTe/CdSe thin film on glass/ITO by electrodeposition at room temperature

SEVDA ILDAN OZMEN[1,*] and HULYA METIN GUBUR[1,2]
[1] Advanced Technology Education Research and Application Center, Mersin University, Mersin 33343, Turkey
[2] Department of Physics, Mersin University, Mersin 33343, Turkey
*Author for correspondence (sevdaildan@mersin.edu.tr)

MS received 7 June 2021; accepted 12 December 2021

Abstract. In this study, a CdTe thin film was formed on glass/indium tin oxide (ITO) substrate at room temperature using electrodeposition. The film was then annealed at 300°C to investigate its effect on the film's optical, morphological, structural and electrical properties. A CdSe thin film was then electrodeposited at room temperature on the annealed p-type glass/ITO/CdTe film. The two films were prepared at room temperature without precursors or additives, using very low concentrations of chemicals. This significantly reduces the cost of production and minimizes its environmental impact. The as-deposited and annealed glass/ITO/CdTe thin film and glass/ITO/CdTe/CdSe heterojunction thin film were characterized using UV–vis spectrometer, scanning electron microscopy, energy-dispersive X-ray spectroscopy, X-ray diffraction and Hall effect measurement system. The results showed that p-CdTe/n-CdSe heterojunction thin film was nanostructured and polycrystalline. This film can be important for solar cells due to its charge carrier density (1.95×10^{20} cm^{-3}), resistivity value (2.42×10^{-3} Ω-cm), and appropriate optical bandgap (1.64 eV) meeting the solar spectrum.

Keywords. Electrodeposition; semiconductor thin film; optical properties; electrical properties; structural characterization.

1. Introduction

Currently, global energy demand stands at 13 TW and is expected to rise by almost 60% by the middle of the century. Owing to the lack of sufficient fossil fuel resources, it is not possible to satisfy this need. Solar energy is thus an attractive source as it is readily available and renewable [1]. In recent years, research has focused on improving the performance of solar cells by using CdTe and CdSe heterojunction techniques. Heterojunction solar cells have p–n junctions that combine two regions of a semiconductor with different concentrations of holes and electrons [2,3].

Semiconductor thin films of II–VI compounds (CdTe, CdSe, CdS, ZnS, etc.) are important in solar cell applications due to their absorption in the visible region of the solar spectrum [4,5]. In particular, CdTe and CdSe semiconductors with a direct bandgap of 1.45 eV [6,7], 1.72 eV [2,8] and high absorption coefficient are highly suitable materials for photovoltaic applications. Just a few micrometres of semiconductor thin film is sufficient to absorb incoming light [9,10]. Essential parameters in the manufacture of photovoltaic semiconductor films include low cost, high performance and easy applicability over large areas [11,12]. A variety of production techniques have been used to obtain CdTe and CdSe thin films, such as spray pyrolysis [13], closed space sublimation [14], thermal evaporation [3,15], chemical bath deposition [8,16] and electrodeposition [17,18]. Among these techniques, electrodeposition is an essential method because the film's morphological, structural and electrical properties can be easily controlled by concentration, pH, temperature, current and potential. In addition, electrodeposition allows control of nanoparticle size [11,19]. While a range of techniques has been used to produce CdTe/CdSe heterojunction solar cells [2,3,12,14,15,20–22], just a few studies [11,17,23–25] have used electrodeposition at room temperature.

Cathodic electrodeposition of CdTe in an aqueous medium is performed in acidic conditions [26–28]. The overall reaction for the formation of CdTe is as follows:

$$Cd^{2+} + HTeO_2^+ + 3H^+ + 6e^- \rightarrow CdTe + 2H_2O$$

The cathodic electrodeposition of CdSe is performed in an aqueous medium in acidic conditions [29]. The overall reaction for the formation of CdSe is as follows:

$$Cd^{2+} + H_2SeO_3 + 4H^+ + 6e^- \rightarrow CdSe + 3H_2O$$

In this study, the p-CdTe/n-CdSe heterojunction was formed using a constant cathodic current density of 1 mA cm^{-2} by the galvanostatic method on glass/indium tin oxide (ITO) substrates at room temperature (25 ± 2°C) without

Published online: 25 April 2022

any additives. The p-CdTe/n-CdSe heterojunction was then characterized in terms of its optical, structural, compositional, morphological and electrical properties.

2. Experimental

The deposition solutions used to form the CdTe and CdSe thin films were prepared with 99% cadmium chloride anhydrous (Acros) for the Cd source, 99% tellurium(IV) oxide (Acros) for the Te source, 98% selenium dioxide (Sigma) for the Se source, 37% hydrochloric acid (Merck) to adjust the pH, and ultrapure water. No precursors or additives were used, such as nitrate [30], Na_2SO_4 [31], $CdCI_2$ and CdF_2 [32–34], 1-butyl-3-methylimidazolium chloride [35], cetyltrimethylammonium bromide (CTAB) [36] for electrodeposition of the thin films.

Electrodeposition was carried out at room temperature using CHI 660D electrochemical workstation with a three-electrode system by the galvanostatic method. An ITO-coated glass (surface resistivity 8–12 Ω sq^{-1}) was used as the working electrode, a platinum sheet was used as the counter electrode and Ag/AgCI (3.5 M KCI) was used as the reference electrode for the electrodeposition set up.

2.1 *Electrodeposition of CdTe and CdSe thin films*

The CdTe thin film was electrodeposited on the ITO/glass substrate in a solution of 0.1 M $CdCI_2$ and 0.1 mM TeO_2, pH adjusted to ∼2 with HCl. A current of 1 mA cm^{-2} was used for 1 h for deposition. The electrodeposition was repeated twice on the same substrate and the electrolyte was refreshed each time. Before and after deposition, the substrate was cleaned with ethanol, propanol, acetone, and ultrapure water, and then dried with an air dryer. Following deposition, the glass/ITO/CdTe thin film was annealed at 300°C in a normal air atmosphere using a Protherm Furnace.

The CdSe thin film was deposited on an annealed glass/ITO/CdTe substrate from a solution of 0.1 M $CdCI_2$ and 0.1 mM SeO_2, pH adjusted to ∼2 with HCl, using a current density of 1 mA cm^{-2}. The electrodeposition was repeated two times for an hour on the same substrate and the electrolyte was refreshed each time. Before the electrodeposition of CdSe on glass/ITO/CdTe, the CdSe films were fabricated on the glass/ITO substrate to determine the appropriate electrodeposition conditions.

2.2 *Characterization of the CdTe and CdTe/CdSe thin films*

The transmission spectra of all the films were measured using a UV–visible spectrophotometer (Shimadzu UV-1700) with a wavelength range of 190–1100 nm. The optical bandgap of the films was determined from the transmission spectra. The X-ray diffraction (XRD) patterns were obtained by the Rigaku Smart Lab X-ray diffractometer using CuKα radiation ($\lambda = 1.54$ Å). The information on the surface morphology of the films was recorded with a Zeiss-Supra 55 FE-SEM (field emission scanning electron microscopy) and the chemical composition of the films was identified with the energy-dispersive X-ray spectroscopy (EDX). The resistivity, carrier concentration and mobility of the films were determined at room temperature in a Van der Pauw four-point probe configuration, using gold contacts with a magnetic induction of 0.54 T by the Hall effect measurement system (HMS-3000).

3. Results and discussion

3.1 *Morphological properties*

The surface properties were analysed using a scanning electron microscope (SEM). Figure 1 shows the SEM images of the as-deposited and annealed glass/ITO/CdTe films at various magnifications. From the images of (a) as-deposited and (b) annealed at 300.00 KX, the grain sizes are around 20–40 nm. After annealing, the grain boundaries have become noticeable, while the grain structures have become more spherical. A smooth, uniform and crack-free surface with spherical grains can also be seen in the SEM images of (c) as-deposited and (d) annealed glass/ITO/CdTe thin films at 50.00 KX magnification. Furthermore, annealing has not introduced any fractures or cracks. By EDX analysis, the atomic percentage of the nanosized glass/ITO/CdTe film was determined. This indicates that the film is rich in tellurium. The atomic percentages of Cd and Te were 41% and 59%, respectively.

Figure 2 shows the surface images of the heterojunction obtained by CdSe deposited on the glass/ITO/CdTe substrate at magnifications of (a) 300.00 KX and (b) 50.00 KX. The glass/ITO/CdTe/CdSe film grain sizes are ∼30 nm, while the film is smoothly covered without any surface pinholes and there are no cracked or broken areas on the surface. The atomic percentages of the film, determined by EDX analysis, are 44% Cd, 53% Se and 3% Te. Figure 3 shows the chemical composition of the CdTe/CdSe thin film. The film is selenium-rich with a small amount of tellurium.

3.2 *Structural properties*

The structural characterization of the nanostructured thin films was determined using XRD. Figure 4 illustrates XRD patterns of as-deposited and annealed glass/ITO/CdTe films. The diffraction peaks of the films matched with the reference cards [37–42] of the Joint Committee on Powder Diffraction and Standards (JCPDS). They were determined to be polycrystalline, consisting of cubic (C) and hexagonal

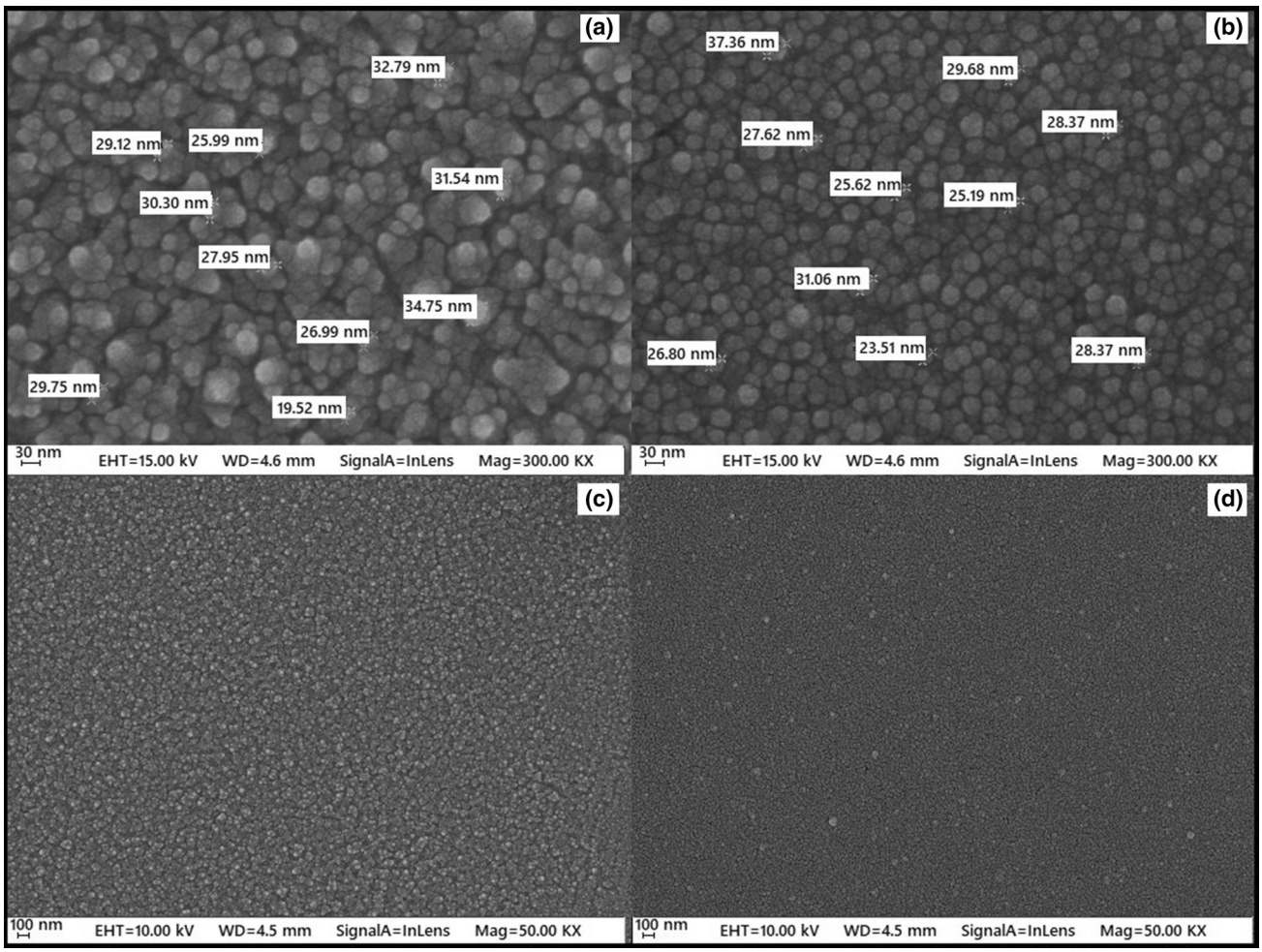

Figure 1. Surface images of (**a–c**) as-deposited and (**b–d**) annealed glass/ITO/CdTe thin films at 300.00 and 50.00 KX magnifications, respectively.

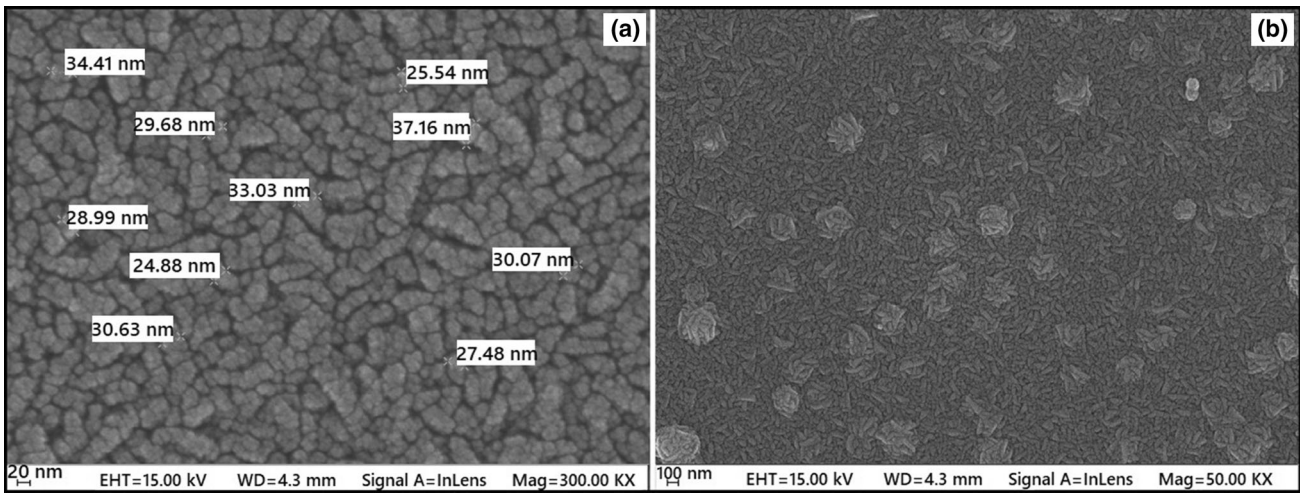

Figure 2. Surface images of glass/ITO/CdTe/CdSe film at (**a**) 300.00 and (**b**) 50.00 KX magnification.

(H) phases. The characteristic diffraction peaks of the as-deposited and annealed films show annealing changes in the structure of the CdTe thin film. Specifically, after annealing in a normal air atmosphere at 300°C, the (111) and (200) peaks of the cubic phase disappear, whereas the intensity of the other peaks increases This increase in

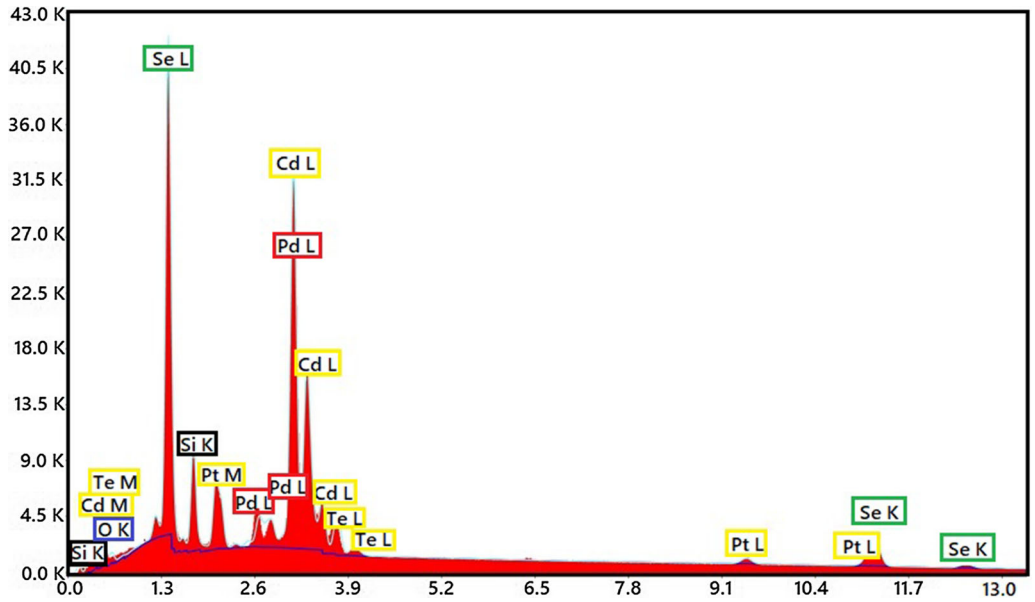

Figure 3. EDX analysis results for glass/ITO/CdTe/CdSe thin film.

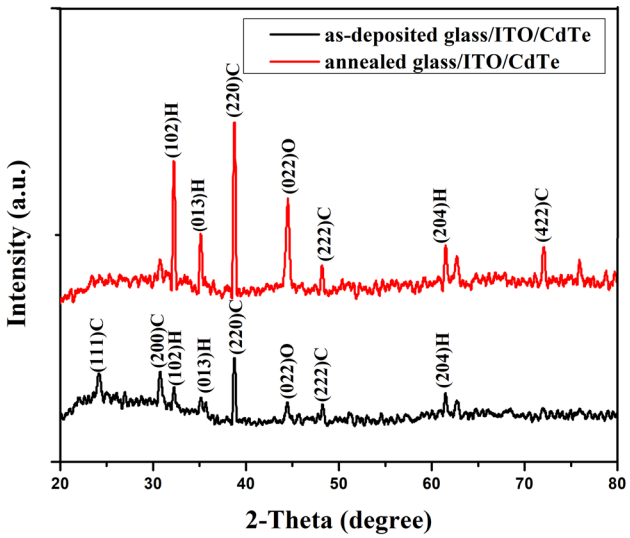

Figure 4. XRD patterns for as-deposited and annealed glass/ITO/CdTe film.

diffraction peak intensity following annealing indicates that the film's crystal structure has been improved.

The following structural properties of the films were investigated: crystallite sizes, dislocation density, the number of crystallites per unit surface area and strain values. The crystallite sizes were calculated using the Scherrer equation,

$$D_{hkl} = \frac{K\lambda}{\beta\cos\theta}, \tag{1}$$

where K is a constant taken as 0.9, β is FWHM (half-maximum width) in radians, λ the wavelength of the X-ray used, and θ the Bragg angle. The XRD data were used to calculate dislocation density ($\delta = 1/D_{hkl}^2$), the number of crystallites per unit surface area ($N = d/D_{hkl}^3$, where d is the film thickness) and strain value ($\varepsilon = \beta\cos\theta/4$). All parameters were calculated for the as-deposited and annealed CdTe film. Table 1 shows the data calculated (220) C diffraction peaks. The same peaks were also investigated in the as-deposited and annealed glass/ITO/CdTe films. This showed that, after annealing, the half-maximum width (FWHM) decreased while the crystal size increased. Consequently, there were reductions in dislocation density, the number of crystallites per unit surface area and film strain.

Figure 5 shows the XRD patterns of the electrodeposited CdSe film on annealed glass/ITO/CdTe. The structure of the CdTe/CdSe was determined by the XRD pattern that corresponded to the JCPDS reference cards [43,44] like a mixed hexagonal and cubic crystal structure. The glass/ITO/CdTe/CdSe film's crystallite size, dislocation density, number of crystallites per unit surface area, and strain value were also calculated with the XRD data. Table 1 shows the determined CdTe/CdSe film parameters using the (002) H diffraction peak.

3.3 *Optical properties*

The films' optical transmission properties were measured at room temperature in the wavelength range of 300–1100 nm. Film thicknesses were calculated by determining the transmission interferences in the transmission spectrum using the following equation:

$$d = \left[\frac{\lambda_1\lambda_2}{2n(\lambda_2 - \lambda_1)}\right], \tag{2}$$

where d is the film thickness, n is the refractive index, and λ_1 and λ_2 are the wavelengths at the two adjacent maxima

Table 1. Structural properties of the as-deposited glass/ITO/CdTe, annealed glass/ITO/CdTe and glass/ITO/CdTe/CdSe films.

	As-deposited glass/ITO/CdTe	Annealed at 300°C glass/ITO/CdTe	As-deposited glass/ITO/CdTe/CdSe
Crystal structure	Cubic		Hexagonal
(hkl)	(220)		(002)
FWHM (deg)	0.15	0.13	0.12
D (nm)	56.55	65.75	67.91
δ (10^{14} line m^{-2})	3.13	2.31	2.17
N (10^{22} m^{-2})	1.28	0.82	1.10
ε (10^{-4})	6.13	5.27	5.10

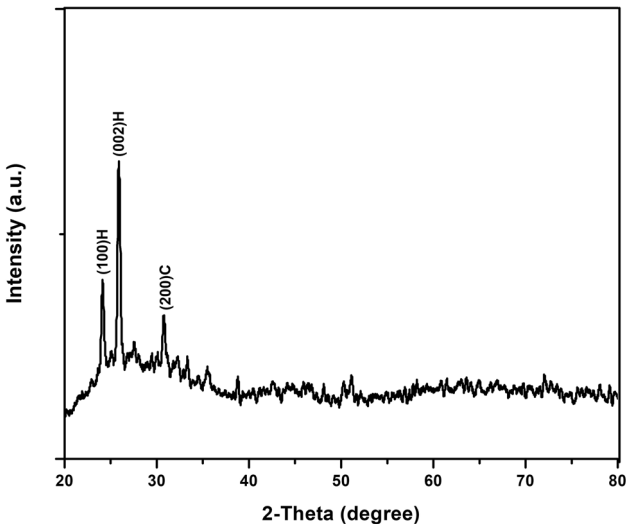

Figure 5. The XRD patterns of glass/ITO/CdTe/CdSe.

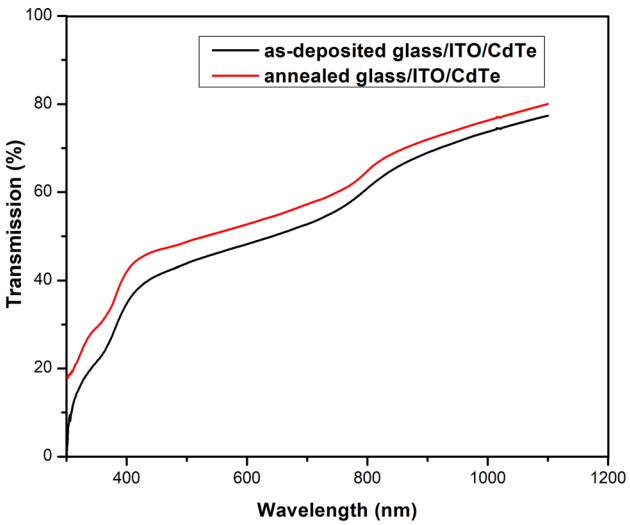

Figure 6. Graph of transmittance (T%) *vs.* wavelength for as-deposited and annealed glass/ITO/CdTe.

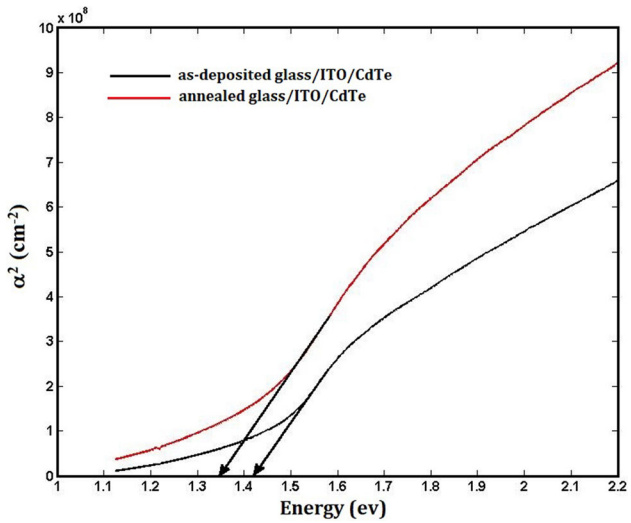

Figure 7. α^2 *vs.* photon energy of as-deposited and annealed glass/ITO/CdTe.

(or minima) [45]. The optical bandgaps (E_g) were determined by the Tauc equation,

$$(\alpha h\nu) = A(h\nu - E_g)^n, \tag{3}$$

where A is a constant parameter, α is the absorption coefficient, $h\nu$ is the photon energy and n indicates the type of optical transitions (n = 1/2 indicates direct transition while n = 2 indicates indirect transition) [46]. n is 1/2 as CdTe and CdSe show direct optical transition. From the plot of $(\alpha h\nu)^2$ *vs.* $h\nu$, the optical bandgap energy (E_g) was found where the linear portions were extrapolated to the energy axis at $\alpha = 0$.

Figure 6 shows the transmission spectrums of the as-deposited and annealed glass/ITO/CdTe films. The thickness of the thin film was calculated to be ~360 nm using equation (2) and figure 6. Figure 7 shows that the E_g of the as-deposited and annealed glass/ITO/CdTe films were 1.42 and 1.35 eV, respectively. According to the expected

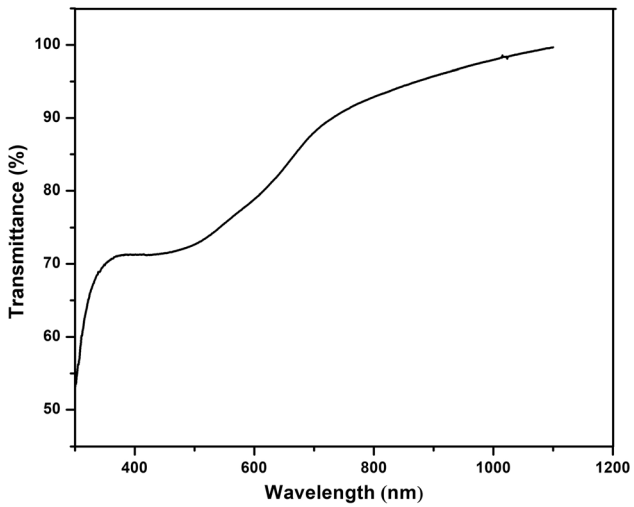

Figure 8. Graph of transmittance (*T*%) *vs.* wavelength for glass/ITO/CdTe/CdSe.

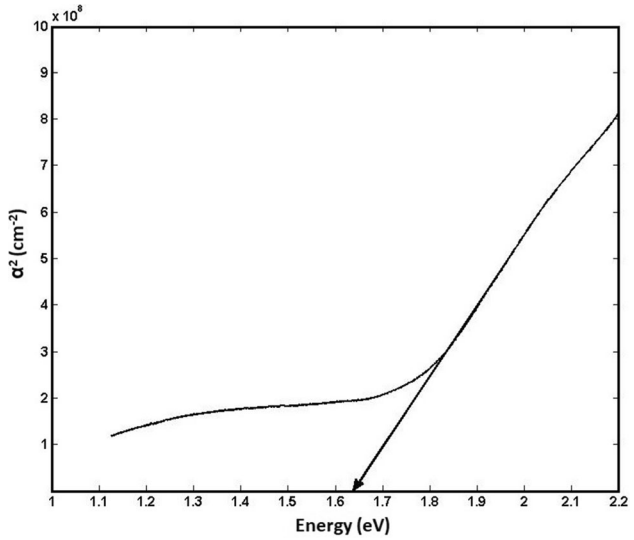

Figure 9. α^2 *vs.* photon energy of glass/ITO/CdTe/CdSe.

classic effect, annealing significantly changed the films' optical properties. This is based on the principle that a film's atoms move to where they can reach the most thermodynamically stable structure under the effect of annealing. In addition, annealing can correct other defects in the solid such as irradiation, surface energy states and voids. We also observed the expected annealing effects. In particular, annealing increased film transmittance and decreased the optical bandgap by about 0.07 eV from the α^2–hv graphs.

We also investigated the optical transmission and optical bandgap of the glass/ITO/CdTe/CdSe thin film. Figure 8 shows the film's transmission spectrum. The film thickness was calculated to be ~440 nm using equation (2) and figure 8. The optical bandgap of the CdTe/CdSe film was determined to be 1.64 eV from figure 9. This value is close to the bandgap of 1.74 eV for bulk CdSe thin film.

3.4 *Electrical properties*

Using the Van der Pauw method, the electrical properties of the films were investigated at room temperature using a Hall effect measurement device. The measurements were performed on four corners of the films by producing ohmic contacts. The magnetic field magnitude and current values were 0.54 Tesla and 1 mA, respectively. The Hall effect measurement provided information about film resistivity (Ω-cm), mobility ($cm^2\ Vs^{-1}$), carrier density (cm^{-3}) values and carrier type using equation (4). The conductivity of semiconductors is given by:

$$\sigma = q\left(n\mu_n + p\mu_p\right), \tag{4}$$

where μ_n and μ_p refer to the mobilities of the electrons and holes, and n and p refer to the density of electrons and holes, respectively. Table 2 shows the resistivity (Ω-cm), mobility ($cm^2\ Vs^{-1}$), carrier density (cm^{-3}) values and carrier type for the as-deposited glass/ITO/CdTe, annealed glass/ITO/CdTe and glass/ITO/CdTe/CdSe films. Following annealing

Table 2. Hall effect measurements of as-deposited glass/ITO/CdTe, annealed glass/ITO/CdTe and glass/ITO/CdTe/CdSe films.

	Glass/ITO/CdTe	Glass/ITO/CdTe	Glass/ITO/CdTe/CdSe
Annealed temperature (°C)	As-deposited	300	As-deposited
E_g (eV)	~1.42	~1.35	~1.64
Carrier density (cm^{-3})	2.15×10^{19}	2.65×10^{20}	1.95×10^{20}
Mobility ($cm^2\ Vs^{-1}$)	5.47×10^{2}	4.55×10^{1}	5.35×10^{1}
Resistivity (Ω-cm)	5.32×10^{-4}	5.17×10^{-4}	2.42×10^{-3}
Carrier type	n	p	n

at 300°C, the carrier type of the as-deposited CdTe changed from n-type to p-type because the film's atoms adopted a more thermodynamically stable structure, as explained above in the section on optical properties. Table 2 also shows that annealing increased the carrier density of the glass/ITO/CdTe but reduced resistivity and mobility. The resistivity of the as-deposited and annealed films were 5.32 $\times$ 10^{-4} Ω-cm and 5.17 $\times$ 10^{-4} Ω-cm, respectively, which was very low compared to previous [11,24,47] studies. Previous studies report n-type single-crystal CdTe carrier concentrations ranging from 6 $\times$ 10^{14} to 2 $\times$ 10^{18} cm^{-3}, depending on high purity and doped [11,48–50]. For high-efficiency solar cells, the carrier density value should be higher than 10^{20} cm^{-3} [51]. In this study, annealing increased the carrier density values for the glass/ITO/CdTe film from 2.15 $\times$ 10^{19} cm^{-3} to 2.65 $\times$ 10^{20} cm^{-3}. The glass/ITO/CdTe/CdSe thin film was determined as n-type, thus obtaining the p–n heterojunction. This is a desirable outcome because we aimed to build a p–n heterojunction with the p-CdTe/n-CdSe film.

4. Conclusions

In this study, room-temperature electrodeposition was used to create glass/ITO/CdTe and glass/ITO/CdTe/CdSe thin films of ~360 and ~440 nm, respectively. The SEM images indicated that the grain sizes of the films were in the range of 20–40 nm with smooth, uniform and crack-free surfaces comprised of spherical grains. The morphological investigations indicated that the CdTe and CdSe nanoparticles were Te-rich and Se-rich, respectively. The films were formed smoothly on the surface without cracks or fractures. The glass/ITO/CdTe thin film obtained by electrodeposition was n-type. The effect of annealing on the CdTe thin film was investigated. Annealing at 300°C in a normal air atmosphere had numerous effects. It converted the film's conductivity from n-type to p-type. In addition, the E_g of the film changed from 1.42 to 1.35 eV, carrier density increased from 2.15 $\times$ 10^{19} to 2.65 $\times$ 10^{20} cm^{-3}, and the polycrystalline structure changed. Finally, the half-maximum width decreased and, the crystal size increased, which decrease the dislocation density, the number of crystallites per unit surface area, and strain. To form the CdTe/CdSe heterojunction, a CdSe thin film was electrodeposited on the glass/ITO/CdTe film. The CdSe thin film was n-type according to electrical measurements. Thus, the p-CdTe/n-CdSe heterojunction was formed and the resistivity of CdTe/CdSe heterojunction thin film was measured as 2.42 $\times$ 10^{-3} Ω-cm. While the E_g of the film was 1.64 eV, which is close to the bandgap of 1.74 eV for bulk CdSe thin film. Taken together, these results demonstrate that a glass/ITO/CdTe/CdSe heterojunction thin film obtained by room-temperature electrodeposition method is a significant material for solar cells with its cost and environmental benefits.

Acknowledgements

This study was supported by the Research Fund of Mersin University in Turkey with Project Number: 2017-2-TP3-2593.

References

[1] Zhu H and Lian T 2012 *Energy Environ. Sci.* **5** 9406
[2] Amin S A, Salim S T, Salam K M A and Galib M A Al 2013 *Int. J. Electr. Energy* **1** 1
[3] Borah M N, Chaliha S, Sarmah P C and Rahman A 2008 *J. Optoelectron. Adv. Mater.* **10** 1333
[4] Manikandana M, Nisha Francisa P, Dhanuskodia S, Maheswarib N and Muralidharanb G 2018 *J. Mater. Sci. Mater. Electron.* **29** 17397
[5] Tian L, Yang H, Ding J, Li Q, Mu Y and Zhang Y 2014 *Curr. Appl. Phys.* **14** 881
[6] Patil V B, More P D, Sutrave D S, Shahane G S, Mulik R N and Deshmukh L P 2000 *Mater. Chem. Phys.* **65** 282
[7] Sisman I and Demir U 2011 *J. Electroanal. Chem.* **651** 222
[8] Oksuzoglu F, Metin Gubur H, Havare A K, Ildan Ozmen S, Unal M and Tozlu C 2020 *J. Photonics Energy* **10** 1
[9] Grätzel M 2006 *Nanocrystalline ınjection solar cells* (eds) J Poortmans and A Vladimir (Hoboken: John Wiley)
[10] Asim N, Sopian K, Ahmadi S, Saeedfar K, Alghoul M A, Saadatian O *et al* 2012 *Renew. Sustain. Energy Rev.* **16** 5834
[11] Mayabadi A, Mirabbaszadeh K, Pawbake A, Rondiya S, Rokade A, Waykar R *et al* 2017 *J. Mater. Sci. Mater. Electron.* **28** 18745
[12] Alam S, Pathan M A K, Siddiquee K A M H, Islam A B M O, Gafur M A, Saha D K *et al* 2013 *Optik (Stuttg)* **124** 2165
[13] Elango T, Subramanian V and Murali K R 2000 *Surf. Coatings Technol.* **123** 8
[14] Li C, Wang F, Chen Y, Wu L, Zhang J, Li W *et al* 2018 *Mater. Sci. Semicond. Process.* **83** 89
[15] David Kumar M M and Devadason S 2013 *Appl. Nanosci.* **3** 453
[16] Metin Gubur H, Septekin F, Alpdogan S and Ildan Ozmen S 2018 *IOSR J. Appl. Phys.* **10** 7
[17] Kim S-H, Lee J-Y, Han W-K and Lee J-H 2010 *Thin Solid Films* **518** 7222
[18] Kim D U, Hangarter C M, Debnath R, Ha J Y, Beauchamp C R, Widstrom M D *et al* 2013 *Solar Cells Sol. Energy Mater. Sol. Cells* **109** 246
[19] Luo H, Ma L G, Xie W M, Wei Z L, Gao K G, Zhang F M *et al* 2016 *Appl. Phys. A Mater. Sci. Process.* **122** 1
[20] Majid F, Malik A, Ata S, Hussain Z, Bibi I, Iqbal M *et al* 2018 *Z. Phys. Chem.* **233** 1
[21] Ju T, Yang L and Carter S 2010 *J. Appl. Phys.* **107** 104311
[22] Baines T, Zoppi G, Bowen L, Shalvey T P, Mariotti S, Durose K *et al* 2018 *Sol. Energy Mater. Sol. Cells* **180** 196
[23] Gurevits J, Bereznev S, Mikli V, Naidu R, Mellikov E and Kois J 2014 *Mater. Res. Soc. Symp. Proc.* **1707** 576

[24] Peksöz A 2016 *Uludağ Univ. J. Fac. Eng.* **21** 1
[25] Li Q, Tian L, Chi K, Yang H, Sun M and Fu W 2013 *Appl. Surf. Sci.* **270** 707
[26] Abdul-Manaf N A, De Silva D S M, Dharmadasa I M, Salim H I, Kumarasinghe K D M S P K and Pathiratne K A S 2016 *Ceylon J. Sci.* **45** 53
[27] Rajeshwar K 1992 *Adv. Mater.* **4** 23
[28] Razmjoo O, Bahrololoom M E and Najafisayar P 2017 *Ceram. Int.* **43** 121
[29] Chévere-Trinidad N L, Gurbuz S, Kramer J and Venkataraman D 2015 *Handbook of Nanoelectrochemistry* Springer International Publishing p 1
[30] Salim H I, Patel V, Abbas A, Walls M and Dharmadasa I M 2015 *J. Mater. Sci. Mater. Electron.* **26** 3119
[31] Bocchetta P, Santamaria M and Di Quarto F 2013 *Electrochim. Acta* **88** 340
[32] Echendu O K, Dejene B F and Hone F G 2018 *Mater. Sci. Eng. B Solid-State Mater. Adv. Technol.* **232–235** 55
[33] Echendu O K, Fauzi F, Weerasinghe A R and Dharmadasa I M 2014 *Thin Solid Films* **556** 529
[34] Osuwa J C and Chigbo N I 2012 *Chalcogenide Lett.* **9** 501
[35] Chauhan K R, Burgess I J, Chang G S and Mukhopadhyay I 2014 *J. Electroanal. Chem.* **713** 70
[36] Fu W, Liu T, Mu Y, Wang J, Li S, Yang L *et al* 2015 *J. Alloys Compd.* **636** 97
[37] Joint Committee on Powder Diffraction Standards–JPDS. *Inorganic Crystal Structure Database Diffraction Data,* PDF Card No: 01-082-0474
[38] Joint Committee on Powder Diffraction Standards–JPDS. *Inorganic Crystal Structure Database Diffraction Data,* PDF Card No: 03-065-1047
[39] Joint Committee on Powder Diffraction Standards–JPDS. *Inorganic Crystal Structure Database Diffraction Data,* PDF Card No: 01-079-3179
[40] Joint Committee on Powder Diffraction Standards–JPDS. *Inorganic Crystal Structure Database Diffraction Data,* PDF Card No: 01-080-0089
[41] Joint Committee on Powder Diffraction Standards–JPDS. *Inorganic Crystal Structure Database Diffraction Data,* PDF Card No: 01-077-7297
[42] Joint Committee on Powder Diffraction Standards–JPDS. *Inorganic Crystal Structure Database Diffraction Data,* PDF Card No: 01-080-0090
[43] Joint Committee on Powder Diffraction Standards–JPDS. *Inorganic Crystal Structure Database Diffraction Data,* PDF Card No: 01-077-7287
[44] Joint Committee on Powder Diffraction Standards–JPDS. *Inorganic Crystal Structure Database Diffraction Data,* PDF Card No: 01-075-5679
[45] Pankove J and Acque I 1971 *Optical processes in semiconductors*. (New York: Dover Publications Inc.)
[46] Metin H, Erat S, Arı M and Bozoklu M 2008 *Optoelectron. Adv. Mater. Rapid Commun.* **2** 92
[47] Miyake M, Murase K, Hirato T and Awakura Y 2004 *J. Electroanal. Chem.* **562** 247
[48] Segall B, Lorenz M R and Halsted R E 1963 *Phys. Rev.* **129** 2471
[49] Takahashi M, Uosaki K, Kita H and Yamaguchi S 1986 *J. Appl. Phys.* **60** 2046
[50] von Windheim J A and Cocivera M 1992 *J. Phys. Chem. Solids* **53** 31
[51] Nishio T, Takahashi M, Wada S, Miyauchi T, Akita K, Goto H *et al Electr. Eng. Japan (English Transl. Denki Gakkai Ronbunshi)* **164** 12